

The LINC-NIRVANA Fringe and Flexure Tracker: Piston Control Strategies

Steffen Rost, Thomas Bertram, Christian Straubmeier, Yeping Wang, Andreas Eckart

I. Physikalisches Institut, University of Cologne, Zùlpicher Str. 77, 50937 Cologne, Germany

ABSTRACT

The Fringe and Flexure Tracking System (FFTS) is designed to correct the atmospheric piston variations and the instrumental flexure during the NIR interferometric image acquisition of the LINC-NIRVANA camera at the LBT. The interferometric image quality depends on the performance of these corrections.

Differential piston and flexure effects will be detected and corrected in a real-time closed loop by analyzing the PSF of a guide star at a frequency of up to several hundred Hz. A dedicated piston mirror will then be moved in a corresponding manner by a piezo actuator.

The FFTS is expected to provide a residual piston of better than 0.1λ at the central wavelength of the science band. Thus, the required correction bandwidth is 10–20 Hz as differential piston simulations of different seeing conditions indicate. Therefore, a sampling frequency of 100–200 Hz is required to correct OPD variations. The upper limit for the loop frequency is the resonance frequency of the mirror and the response function respectively.

The piston mirror as the actuator and the FFTS detector as the sensor feedback are embedded in a very complex system. Many control loop aspects like sampling frequencies, delays, controller algorithm and control bandwidth have to be identified. With accurate simulations of the system the limits of atmospheric and instrumental conditions for reliable closed loops can be determined against the respective control parameters. We present strategies for the closed-loop control of the piston correction which are suitable to achieve the 0.1λ requirement and the optimal overall imaging performance with a sufficient "all-purpose" control stability.

Keywords: LBT, LINC-NIRVANA, Fringe Tracking, Closed-loop Controller, Piston Correction, OPD, Control

1. INTRODUCTION

The Large Binocular Telescope¹ with its two 8.4 m telescopes on a common mount, allows for a unique combination of high angular resolution, large field of view (FoV), and the sensitivity of a 110 m² light collecting area. It forms the bridge from current 8-10 m class telescope to future giant telescope technology. LINC-NIRVANA² (Fig. 1), the NIR interferometric imaging camera for the LBT incorporates the advantages provided by the LBT design. Because it obeys specific geometric constraints that constitute a Fizeau interferometer, LINC-NIRVANA can profit from the resulting large FoV in two ways: It allows for a virtually unlimited interferometric science FoV (limited by the cost of NIR focal plane arrays). And it allows to exploit the FoV to choose from a large pool of off-axis reference stars for adaptive optics and fringe tracking. In its final expansion stage, LINC-NIRVANA will be equipped with a multi-conjugate adaptive optics system (MCAO) that can gather the light of reference stars in a 6 arcminute diameter field. In terms of angular resolution LINC-NIRVANA will outperform the imaging capabilities of existing 8-10 m class telescopes by a factor of ~ 3 .

The Fringe and Flexure Tracking System (FFTS) is an integral part of LINC-NIRVANA. Its purpose is the realtime detection and compensation of differential piston between the two interferometric channels and the correction of misalignment due to instrumental flexure. A more comprehensive view on the FFTS can be found in Straubmeier et al.⁴

Send correspondence to S. Rost: E-mail: rost@ph1.uni-koeln.de, Telephone: +49 (0)221 470-3548

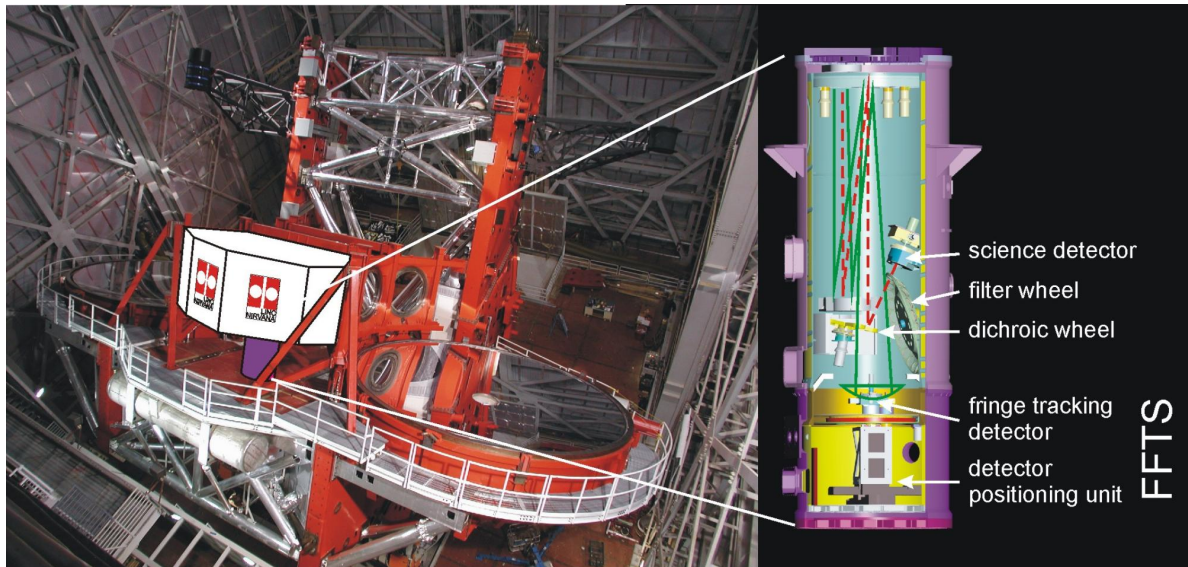


Figure 1. LINC-NIRVANA will be installed in one of the interferometric focal stations of the LBT. The two beams of the interferometer will be combined by a cassegrain telescope within the dewar of LINC-NIRVANA. The fringe tracker is located at the bottom end of the dewar,³ close to the science detector. A set of dichroic beam splitters will reflect part of the NIR spectrum in the center of the science FoV to the science detector. The remaining NIR radiation in the center is transmitted to the fringe tracker. In the FoV exceeding the central 10 arcsec. covered by the science detector, the full NIR spectrum is available to the fringe tracker.

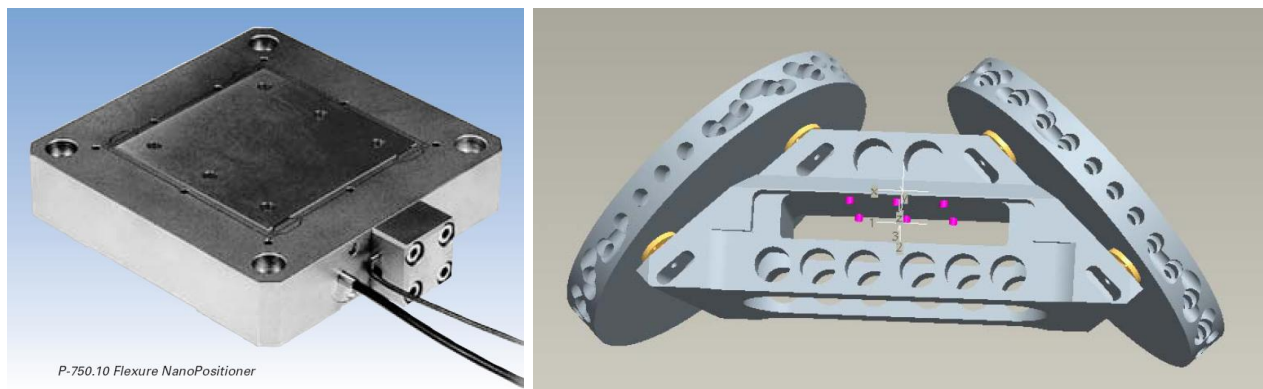


Figure 2. The piezo-driven actuator (left) is mounted in the center of gravity of the piston mirror (right). The design of the frame shows high stiffness and minimum weight, resulting in optimized dynamics of the system.⁵

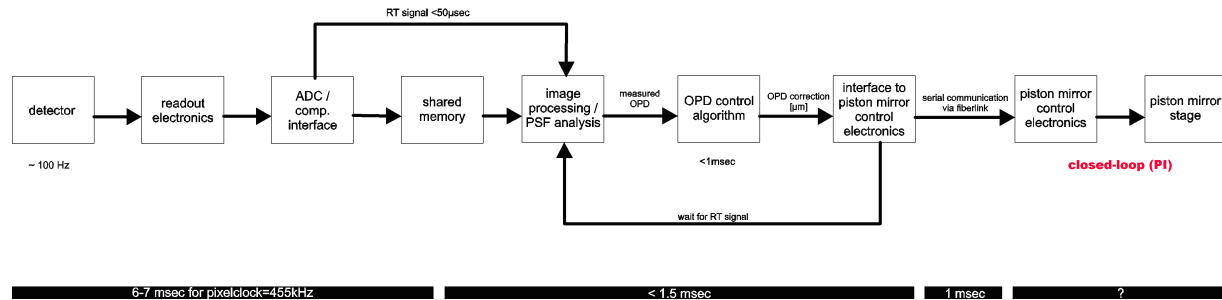


Figure 3. The FFTS control loop and latencies. The control signal is distorted by a low sampling rate (~ 100 Hz), high latency (~ 6 ms) and high noise.⁶ This is compensated in the OPD (optical path difference) control algorithm to some extent. The actuator, i.e. the piezo stage and piston mirror, is driven in closed-loop and limited by the transfer function of the system.

Table 1. Residual piston RMS at the fringe tracking wavelength required to achieve an RMS value of $0.1 \lambda_{\text{Science}}$.

λ_{Science}	Fringe tracking band				
	J	J+H	H	H+K	K
J	0.100	0.085	0.076	0.063	0.057
H	0.132	0.112	0.100	0.083	0.075
K	0.176	0.150	0.133	0.111	0.100

2. REQUIREMENTS

The sky coverage of LINC-NIRVANA is closely related to the performance of the fringe tracking system.⁶ A residual piston of 0.1λ for the central wavelength of the science band is demanded for the FFTS. The performance in turn is related to many parameters, as we show in the following. Table 1 lists the required fringe tracking residual piston for the 0.1λ criterion in the science band.

The piston error budget due to the control loop effects is analyzed with a simulation of the expected system response. With a detailed model a controlling strategy and parameters can be optimized. On the other hand the limiting reference star magnitude and distance to the target can be estimated if a residual piston performance is specified.

3. DYNAMIC MODEL

The actuator of the FFTS loop is the piston correction mirror mounted on a piezoelectric-driven stage (Fig. 2). The stage is a *P-750* from manufacturer PI with a travel range of $75 \mu\text{m}$. The integrated feedback sensor provides subnanometer resolution and stability in a closed-loop operation. When the momentary differential piston is identified with the FFTS detector the according position for the mirror is established through a PI(D)-controller, which is optimized to the mirror load and temperature drifts, mechanical relaxation over time etc. The dependency on temperature and tilt of the telescope is regarded by look-up tables. This is what we call the “inner loop”. The performance of the FFTS loop strongly depends on the linearity, precision, bandwidth and stability of the inner loop, because there is no precise feedback of the residual piston to the FFTS loop: the piston signal is delayed and disturbed by the FFTS detector SNR and with it the PSF-fitting noise.⁶

Figure 4 shows the measured step and frequency response (bode plot) of a piezo stage without load and with additional piston mirror load in comparison. A first resonance peak is visible at about 150 Hz. For the simulation of the system transient dynamic a parametric model has been obtained with the Matlab System Identification toolbox:

$$H_{\text{piezo}}(s) = e^{-\tau_d s} \frac{0.01236s^4 - 0.04475s^3 + 0.06266s^2 - 0.0403s + 0.01009}{s^5 - 4.834s^4 + 9.418s^3 - 9.241s^2 + 4.565s - 0.9084}, \quad (1)$$

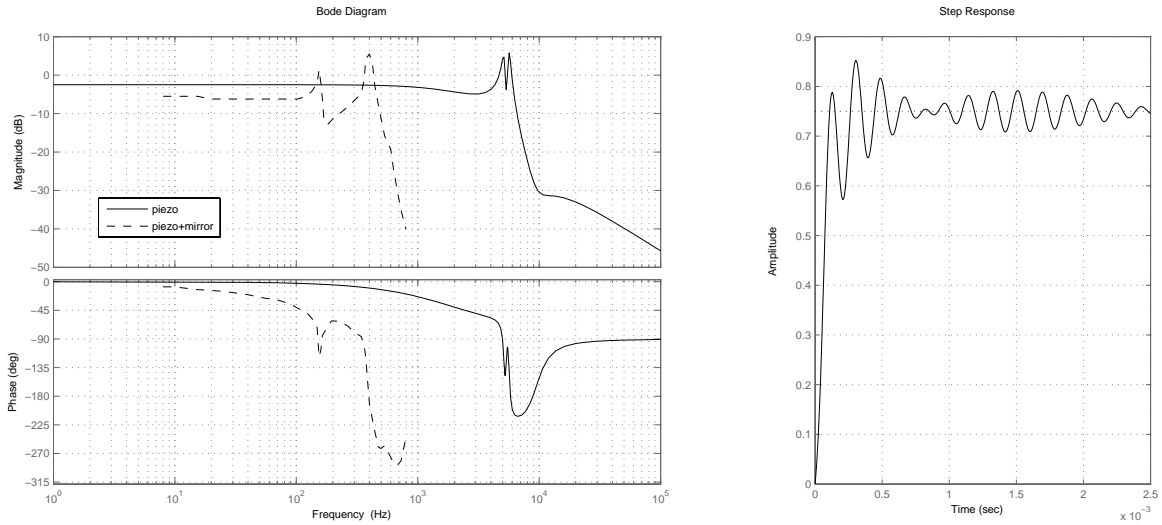


Figure 4. The frequency response of the piezo-driven system depends strongly on the load mass. A pure piezo stage has a much higher resonance frequency than a one with an additional load. First measurements were done with a dummy load corresponding to the mirror mass and show a resonance peak at ~ 150 Hz.

whereas τ_d is the delay of the system ($\tau_d \sim 100 \mu s$). With the Pade approximation of the delay this can be written:

$$H_{\text{piezo}}(s) = H_{\tau_d}(s) \cdot H(s), \quad (2)$$

This is a first model of the combined actuator and piston mirror load and is used in the following for simulations of the systems response. The control parameters of the inner loop with the transfer function:

$$H_{\text{PID}}(s) = \frac{Ds^2 + Ps + I}{s + C}, \quad (3)$$

are currently optimized to a fast and stable system response. In addition a voltage amplifier between the controller and the piezo stage is used. This leads to the inner loop system:

$$G(s) = H_{\text{PID}}(s) \cdot H_{\text{Gain}}(s) \cdot H_{\text{piezo}}(s), \quad (4)$$

At the moment efforts are being made to obtain a more detailed model with measurements (step- and frequency response) of the actual piston mirror.

Figure 5 shows a Simulink model for the FFTS control loop. The OPD (optical path difference) due to the atmospheric conditions are simulated with a seven layer atmospheric model. For a detailed overview on the simulations probing standard and extreme cases see Bertram et al.⁶ In the following atmospheric conditions with a seeing of 1.5", 0.7" and 0.3" are assumed. The OPD time series over 6 seconds is then resampled with the corresponding framerate of the FFTS-detector and a delay is added, due to the detector read-out, A/D-conversion, OPD algorithm CPU-time, etc.

4. DISTURBANCES

4.1. Sampling Rate

The OPD is measured with the FFTS-detector at a fixed framerate which is limited by the magnitude of the reference star. The SNR of the PSF has a strong impact on the piston analysis performance and requires therefore

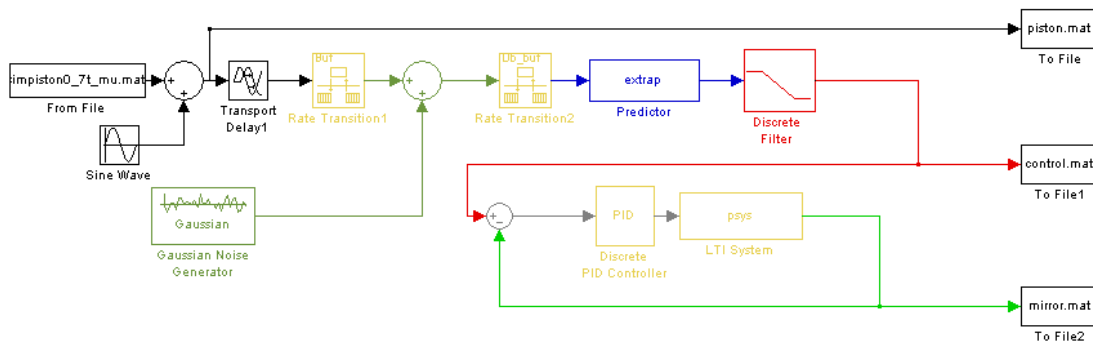


Figure 5. Simulink model for the simulation of the control loop performance with different atmospheric conditions and disturbances from sampling effects, latencies, PSF-fit noise and telescope vibrations.

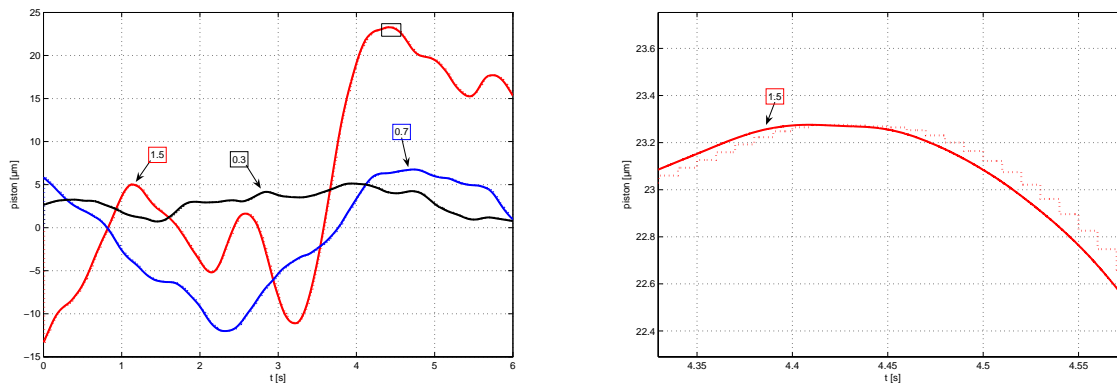


Figure 6. Simulation of the differential piston at different atmospheric conditions: seeing is 1.5", 0.7" and 0.3" respectively. A bad seeing results mainly in a higher piston stroke and faster variations.⁶ To the right in a zoomed view the sampled signal with a sampling rate of 100 Hz and a delay of 8 ms (estimated latency for the FFTS) is visible.

a minimum exposure time. The achieved framerate with a image size of 32×32 pixels is 100-200 Hz (cf. Fig. 6). The piston power spectrum which can be corrected is therefore limited to the Nyquist frequency (50-100 Hz). With no knowledge of the behaviour of the piston in between the samples, the FFTS performance will decrease with lower sampling rates (Fig. 7).

Because of the integration time of the PSF image acquisition, the read-out time and A/D-conversion the piston signal is also delayed. In figure 3 the estimated latencies during the analysis of the piston are noted, wich sums up to a delay of $\tau_s \sim 8$ ms. For stable control the latency should be kept as small as possible, but also a constant delay is desired. Wang et al.⁷ examined the latency variance on a real-time computer system and introduced a software solution for fast and stable data processing.

4.2. PSF Fitting

Bertram et al.⁶ developed a image analysis concept with a multidimensional PSF-fitting algorithm. Differential piston can be determined even with a low Signal-to-Noise ratio. However the goodness of fit will decrease with decreasing SNR, which in turn is dominated by the detector read-out noise. Thus the framerate of the detector is a

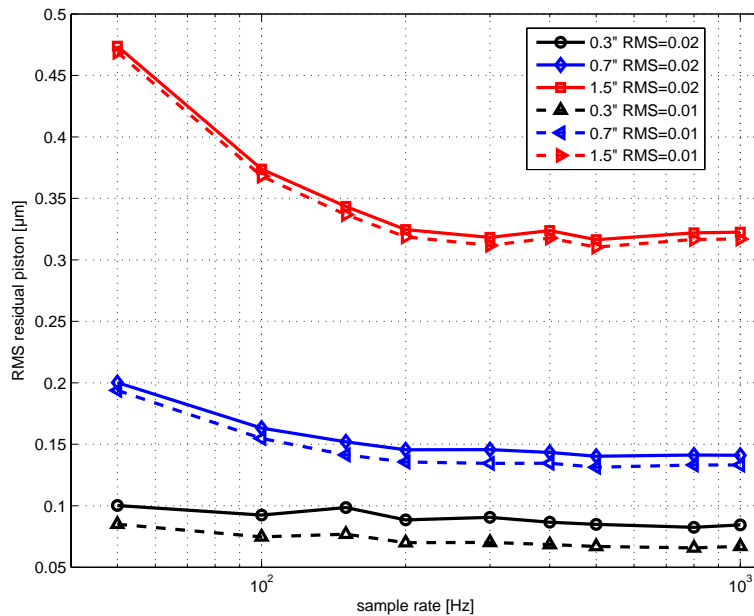


Figure 7. The residual piston as function of the detector frame rate. A PSF-fitting noise of 0.01 μm RMS and 0.02 μm RMS respectively is assumed.

tradeoff between sampling rate and error of the piston signal. As the sampled signal is also delayed, extrapolation or prediction performance is important. With increasing noise due to the fitting, the prediction becomes difficult. This can be compensated with filtering and improved with an adapted filter, when the noise spectrum is known (Fig. 8).

4.3. Telescope Vibration

The LBT is a very complex system. Differential piston can arise in a number of locations. Vibrations of the two arms of the interferometer may be induced by system components such as cooling pumps and fans, as well as by the environment. Although the telescope dome is decoupled from the frame, wind excitation is always evident. The piston power spectrum due to vibrations is not known yet. Currently metrological concepts are developed for vibration measurements of the so far completed parts of the telescope. For first simulations a second order noise spectrum is assumed:

$$H_{\text{vib}}(s) = \frac{A_0 \cdot \omega_0^2}{s^2 + 2Q_f s + \omega_0^2}, \quad (5)$$

with a damping factor $Q_f \sim 0.7$ of the frame and a corner frequency $\omega_0 \sim 1$ Hz. In figure 9 the effects of differential vibration on the residual piston are visible. Both maximum frequency and amplitude are limited by the sampling rate and the latency of the image acquisition.

5. CLASSICAL CONTROL APPROACH

The primary objective of the control design is to achieve precise tracking of almost arbitrary input signals with high control bandwidth in spite of external disturbance. In classical feedback control systems robustness is handled by phase and gain margins. The control signal and the residual piston can be improved with a simple predictor. After the PSF fitting algorithm the signal is resampled to a higher sampling rate (e.g. 1 kHz). By evaluating the derivative for the last n samples the trend of the piston can be extrapolated. The extrapolation also takes care of the latency by evaluating the time $t + \tau_s$. The resulting discontinuities can be compensated with

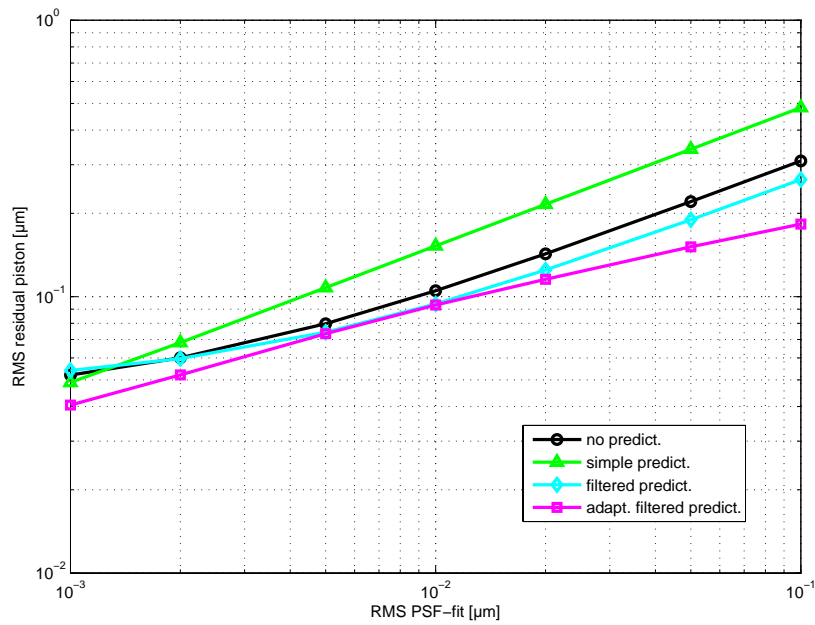


Figure 8. Log-log plot of the RMS of the residual piston against the RMS of PSF-fitting noise. The simulated seeing is $0.3''$ and the detector framerate is 100 Hz.

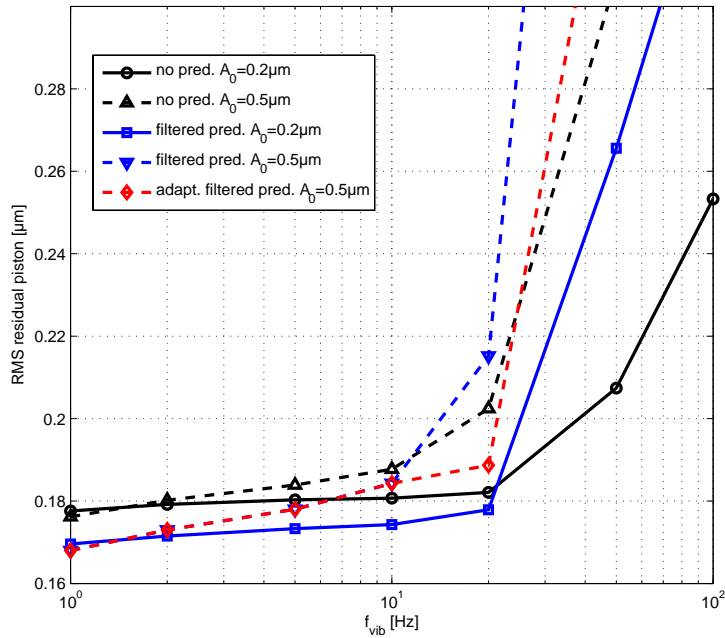


Figure 9. Logarithmic plot of the RMS of the residual piston against the frequency of telescope vibration for different control approaches. The simulated seeing is $0.7''$ and the detector framerate is 100 Hz. A PSF-fit noise of $0.02 \mu\text{m}$ is assumed.

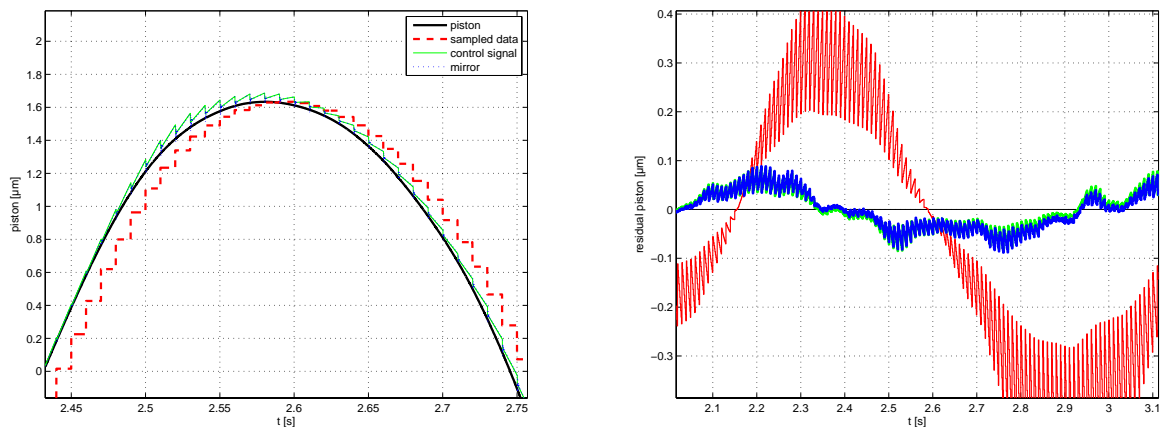


Figure 10. A predictor approach for the control signal improves the control performance, the residual piston (right) is decreased.

a discrete (lowpass) filter. Figure 10 shows that this approach can improve the control performance significantly for the case of a undisturbed signal.

If details and constraints of the disturbances are known, this knowledge of the system can be used to find the optimal configuration. The filter can be adapted to the piston power spectrum. If environmental conditions and instrumental vibrations can be identified, optimized parameters could be stored in corresponding lookup tables.

6. OPTIMIZED CONTROLLERS

The overall residual piston performance is effected by numerous parameters. We presented a first model and control approach for simulations of the system performance against the detector framerate, the PSF-fitting performance and instrumental induced piston. By first tuning the inner loop and advancing the piston mirror model we can focus on the robustness and stability while optimizing the FFTS control loop algorithm. At the moment efforts are being made to collect the nessecary data by:

- fine-tuning the model by analysing the real response of the system in a laboratory setup, providing also the opportunity of in-system designing of controllers
- obtaining the instrumental piston power spectrum with measurements of the telescope vibrations

Constraints on the parameters and uncertainties of the transfer functions:

$$H_{\text{vib}}(s) \cdot H_{\text{SR}}(s) \cdot H_{\tau_s}(s) \cdot H_{\text{fit}}(s) \cdot H_{\text{filter}}(s) \cdot (H_{\text{PID}}(s) \cdot H_{\text{Gain}}(s) \cdot H_{\text{piezo}}(s)) \quad (6)$$

can be derived which leads to a uncertainty model of the system. An optimal controller in the sense of robustness and stability can then be found, e.g with the H_{∞} -approach^{8,9} of the Matlab robust control toolbox.

REFERENCES

1. J. M. Hill, R. F. Green, and H. J. Slagle, "The Large Binocular Telescope," in *Proceedings of the SPIE, paper [6267-18]*, 2006.
2. T. M. Herbst, A. Eckart, R. Ragazzoni, and G. P. Weigelt, "Beyond the fringe: an update on the construction of LINC-NIRVANA, a Fizeau imaging interferometer for the LBT," in *Proceedings of the SPIE, paper [6268-72]*, 2006.

3. W. Laun, H. Baumeister, and P. Bizenberger, "The LINC-NIRVANA IR cryostat," in *Proceedings of the SPIE, paper [6269-190]*, 2006.
4. C. Straubmeier, T. Bertram, A. Eckart, S. Rost, Y. Wang, T. M. Herbst, R. Ragazzoni, and G. P. Weigelt, "The imaging fringe and flexure tracker of LINC-NIRVANA: basic opto-mechanical design and principle of operation," in *Proceedings of the SPIE, paper [6268-55]*, 2006.
5. "LINC-NIRVANA Final Design Review [http : //www.mpia.de/LINC/content/html/fdr.htm](http://www.mpia.de/LINC/content/html/fdr.htm)," tech. rep., 2005.
6. T. Bertram, C. Arcidiacono, C. Straubmeier, S. Rost, Y. Wang, and A. Eckart, "The LINC-NIRVANA fringe and flexure tracker: image analysis concept and fringe tracking performance," in *Proceedings of the SPIE, paper [6268-138]*, 2006.
7. Y. Wang, T. Bertram, S. Rost, C. Straubmeier, and A. Eckart, "The LINC-NIRVANA fringe and flexure tracker: Linux real-time solutions," in *Proceedings of the SPIE, paper [6274-65]*, 2006.
8. S. Skogestad and I. Postlethwaite, *Multivariable Feedback Control*, John Wiley & Sons, 1996.
9. B. M. Chen, T. H. Lee, C. C. Hang, Y. Guo, and S. Weerasooriya, "An H^∞ almost disturbance decoupling robust controller design for a piezoelectric bimorph actuator with hysteresis," *IEEE Trans. Contr. Syst. Technol.* **40**, 1999.